BOREAL ENVIRONMENT RESEARCH 23: 83–103
ISSN 1797-2469 (online)

Helsinki 23 February 2018

A descriptive analysis of the linkage between the vertical stratification and current oscillations in the Gulf of Finland

Irina Suhhova*, Taavi Liblik, Madis-Jaak Lilover and Urmas Lips

*Tallinn University of Technology, Department of Marine Systems, Akadeemia 15A, EE-12618 Tallinn, Estonia (*corresponding author's e-mail: irina.suhhova@ttu.ee)*

Received 20 Apr. 2017, final version received 14 Jan. 2018, accepted 16 Jan. 2018

Suhhova I., Liblik T., Lilover M.-J. & Lips U. 2018: A descriptive analysis of the linkage between the vertical stratification and current oscillations in the Gulf of Finland. *Boreal Env. Res.* 23: 83–103.

The data from five ADCP deployments with duration from one to several months in various locations of the Gulf of Finland were analyzed. The observations revealed that the shear maxima of current velocity were strongly linked to the pycnoclines — the seasonal thermocline or vertical salinity gradient. The shear maxima were not detected when the quasi-permanent halocline temporarily vanished in winter due to strong SW winds causing reversed estuarine circulation in the gulf. The kinetic energy spectra of currents revealed the energy maxima at a broad semi-diurnal frequency band, broad diurnal frequency band, and low-frequency seiches band. In the periods of strong wind forcing and weak stratification, the current oscillations coincided with different modes of seiches. During the periods of the two- or three-layer flow in summer, the inertial oscillations were dominating in the upper layer while seiches could be more prominent either in the upper layer or the halocline.

Introduction

The Gulf of Finland is an elongated estuarine basin, located in the northeastern part of the Baltic Sea (Fig. 1). The gulf is about 400-km long and 48–135-km wide, its average and maximum depths are 37 and 123 m, respectively (Alenius *et al*. 1998). Depth decreases from the entrance to the easternmost part. The average riverine discharge to the gulf, concentrated in its eastern part, is about 3500 $m^3\ s^{-1}$ (Bergström and Carlson 1994). The surface salinity decreases from the entrance to the east from 5–7 g kg^{-1} to 0–3 g kg^{-1} while the deep layer salinity exceeds 8–10 g kg^{-1} (Alenius *et al*. 1998). The typical estuarine circulation pattern with an outflow of fresher water in the upper layer and inflow of saltier water in the deep layer exists in the gulf. The estuarine circulation is intensified by the northeasterly and northerly winds (Elken *et al*. 2003, Liblik and Lips 2011), while, in the case of strong westerlies, it can be altered or even reversed (Elken *et al*. 2003). Furthermore, Elken *et al*. (2014) have found that the recent increase in the frequency of circulation reversals could be caused by a shift in the wind regime with increased frequency of westerly–southwesterly winds in wintertime.

Vertical stratification in the gulf is variable and exhibits a clear seasonality. In winter, the water column in deep enough areas has mostly two-layer structure with a well-mixed upper layer extending from the sea surface until the halocline at the depths of 60–80 m (e.g., Alenius *et al*. 1998). However, considerable haline stratification may appear in the upper layer during calm periods (Liblik *et al*. 2013), and intensive rever-

Editor in charge of this article: Kai Myrberg

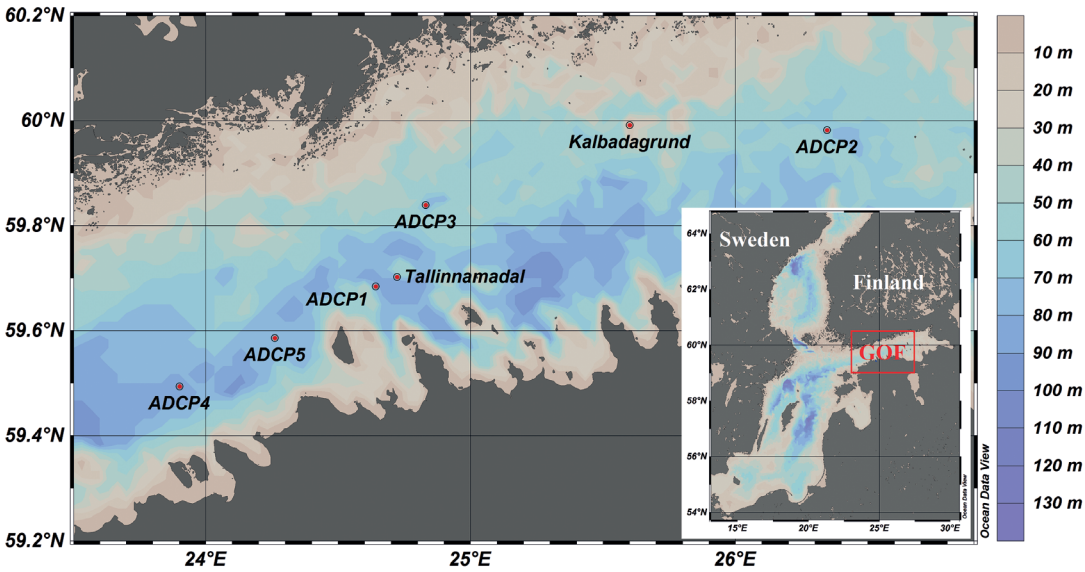

Fig. 1. Map of the study area in the Gulf of Finland. Locations of ADCP deployments (Table 1) and wind measurement locations in Kalbådagrund and Tallinnamadal Lighthouse are shown.

sals of estuarine circulation may cause occasional stratification collapse events (Liblik *et al*. 2013, Elken *et al*. 2014). As a result, three-, two- and one-layer stratification regime may occur in the gulf in winter. In summer, mostly a three-layer vertical structure exists as the seasonal thermocline develops at the depths of 10–30 m (e.g., Alenius *et al*. 1998, Liblik and Lips 2017).

Based on ten series of current profile recordings covering all seasons, Lilover *et al*. (2017) reported that, on average, an inflow with nearly uniform speed throughout the entire water column existed in the deep central part of the gulf in winter, while a layered flow structure was a typical pattern in summer. The vertical structure of currents seems to be linked to the presence and location of the seasonal thermocline (Suhhova *et al*. 2015) and halocline (Liblik *et al*. 2013) while, on the other hand, the changes in circulation are reflected in the variability of vertical stratification (Liblik and Lips 2012). Thus, there should exist a strong interplay between the currents and stratification in the gulf.

Since the gulf is relatively wide, the general circulation may exhibit a transverse structure. As it was suggested already by Palmén (1930) and confirmed by numerical simulations (e.g., Andrejev *et al*. 2004), a quite persistent outflow exists in the surface and sub-surface layers in the northern gulf. As a result, the general (residual) surface circulation is suggested to be cyclonic, but the occurrence of some sub-cells has been shown by model experiments (e.g., Andrejev *et al*. 2004, Elken *et al*. 2011). Lips *et al*. (2017) suggested that in weakly stratified conditions (in winter), the flow structure might correspond to the circulation pattern either driven by spatially uniform longshore wind in lakes (e.g., Bennet 1974, Winant *et al*. 2014) or formed due to the mixing asymmetry in tidal estuaries (Burchard *et al*. 2011). The three-layer flow observed in some summers could correspond to the flow pattern in the relatively deep fjords where the mixing due to tidal currents does not occupy the whole water column (Valle-Levinson *et al*. 2014). In most of these suggestions, the vertical mixing due to current oscillations is assumed to be involved. Thus, it needs to be studied, what are the most energetic current oscillations in different forcing and stratification conditions.

The energy maxima of current oscillations in the Gulf of Finland are usually revealed at a broad semi-diurnal frequency band (BSD), broad diurnal frequency band (BD) or low-frequency seiches band (LFS) (Wübber and Krauss 1979, Jönsson *et al*. 2008, Lilover *et al*.

2011). The seiches with periods of 11, 13 and (17) h together with the inertial motions (period 13.9 h) and semi-diurnal tidal constituents S2 (12.0 h) and M2 (12.42 h) contribute to the BSD band kinetic energy. Seiches with periods of 19 (20) h (4th mode), 24 (22) h (3rd mode) and 28 (26) h (2nd mode) and diurnal tidal constituents K1 (23.93 h) and O1 (25.82 h) are the contributors into the BD frequency band. Note that the periods of seiches are cited here according to Wübber and Krauss (1979) model, without parenthesis, the numbers belong to the entire Baltic and with parentheses to the western Baltic–Gulf of Finland oscillating system. The period of the first mode seiche is 31 hours, and it belongs to the LFS band. Although the occurrence of current oscillations at the listed frequency bands in the Gulf of Finland is known, we lack the knowledge on the vertical distribution of current oscillation energy.

This study aims to examine the concurring variability of currents and thermohaline fields using ADCP (Acoustic Doppler Current Profiler) and CTD (Conductivity, Temperature, and Depth) measurements in the Gulf of Finland. We use five ADCP current profile time series, with duration from one to five month, acquired at different sites of the gulf in 2010–2014. We examined the following hypotheses: (1) one-, two- and three-layer flow regimes can occur in the gulf depending on the wind forcing, (2) strong current shear is linked to the two pycnoclines, and (3) there are differences in the kinetic energy spectra in different layers when a layered flow structure has been realized.

Material and methods

Two out of five current measurement series analyzed in the present paper were acquired in summers 2010 and 2011 (moorings ADCP1 and ADCP3, respectively). Mooring ADCP2 was deployed during the decay of stratification in autumn 2010. Two last deployments (ADCP4 and ADCP5) describe the conditions with the weak seasonal stratification in winter and its strengthening in spring of 2012 and 2014.

A bottom-mounted ADCP (Workhorse Sentinel, Teledyne RDI, 300 kHz) was deployed at five locations (*see* Fig. 1) for the periods of 29 to 148 days (Table 1). Current velocity profiles were measured over 2-m depth bin with the sampling interval of 10 minutes and 30 minutes (for ADCP4) as averages of 50 pings. The sea depth in the deployment locations varied from 67 to 91 m. Due to the surface side lobe effect and ADCP ringing distance, the current velocities were available in the depth range from 62–86 m to 8–10 m, depending on the depth of deployment locations.

CTD profiles acquired using an Ocean Seven 320plus CTD probe (Idronaut S.r.l.) during several cruises were applied as background data on vertical stratification.

Wind data from the Kalbådagrund meteorological station (Finnish Meteorological Institute) — a lighthouse in the central part of the Gulf of Finland (Fig. 1) were used to describe the local atmospheric forcing conditions from June 2010 until September 2011. The wind speed and direction measured at the height of 32 m were available every third hour as a 10 min average. For the two last measurement periods, wind data from the Tallinnamadal Lighthouse were used. Wind speed and direction were measured at the height of 36 m above the sea level and were reported every hour as a 5 min average. To convert the measured wind speed to the standard 10 m height wind speed, the measured values

Table 1. Mooring positions, deployment periods and depth ranges.

Deployment	Longitude (E)	Latitude (N)	Period	Bin depth range (m)	Sea depth (m)
ADCP1	24°37.5´	59°41.0´	1.06.2010–31.08.2010	9–79	84
ADCP2	26°20.8´	59°58.8´	30.09.2010–28.10.2010	8–62	67
ADCP3	24°49.9´	59°50.3´	13.07.2011–05.09.2011	9–73	78
ADCP4	23°54.1´	59°29.6´	21.12.2011–09.05.2012	10–86	91
ADCP5	24°15.6´	59°35.1´	9.12.2013–06.05.2014	10–82	87

were multiplied by a height correction coefficient (0.91 and 0.90, respectively for Kalbådagrund and Tallinnamadal; Launiainen and Saarinen 1984). The relationship between the wind and current velocity during selected measurement periods is characterized in the paper by the complex vector correlation coefficient according to Kundu (1976).

The quality of the current velocity data was checked following the procedure developed by Book *et al*. (2007). The time-series were smoothed with a 1-h moving average filter to get hourly average values. For the low-frequency analysis, all series were smoothed with a 36-h cutoff Butterworth (1930) filter. Time series of the vertical distribution of current velocity components and polar histograms of currents were analyzed based on the hourly average data. Current shear was calculated between the two nearest velocity horizons over the depth range of 2 m using low-pass filtered data. We defined the following criterion based on the current shear square (S^2): if $S^2 < 2 \times 10^{-4}$ s^{-2}, a homogeneous flow is present, if $S^2 > 2 \times 10^{-4}$ s^{-2}, a layered flow is present.

For spectral structure investigations of current oscillations, rotary spectral analysis technique (e.g., Emery and Thomson 2004) was applied to hourly average current data. Dividing time series into two equal-length segments and using 50% overlapping between them the calculated spectrum had 6 degrees of freedom (DoF). To increase the accuracy of the power spectral density at a given depth, an average spectrum over the depth range of 10 m (average of 5 closest spectra) was calculated. As a result, the calculated spectra had 30 DoF. Current speed amplitude was defined as the root mean square of $\sigma^2(f_c) \approx S_c \Delta f$, where $\sigma^2(f_c)$ is the signal variance in a frequency band Δf centered at the frequency f_c, and S_c is the power spectral density (Emery and Thomson 2004).

Power spectral density (PSD) is usually plotted in coordinates log$S(f)$ versus log(f), where $S(f)$ is the power spectral density and f the frequency. Such presentation is useful if the spectral slope has to be estimated. We use another spectral plot in the present paper, namely $fS(f)$ versus log(f) which is a variance-preserving form of spectral presentation. In this presentation, the energy in every frequency interval is proportional to the corresponding area under the spectral line. The use of the linear scale instead of a logarithmic scale of PSD enables to illuminate the depths and frequencies with elevated kinetic energy.

Results

General description of wind, stratification, and currents

Strong seasonal thermocline was observed at 15–25 depth during both summer deployments in 2010 and 2011. The thermocline weakened and deepened from 25–30 m to 40–50 m depth during the measurement period in September-October 2010 (ADCP2). During both measurement periods in winter–spring 2011/2012 and 2013/2014, weakly stratified conditions prevailed in December–January, but later, vertical stratification developed and three-layer stratification pattern existed by the end of both deployments.

The average wind speed of the first deployment was 5.8 m s^{-1}, and the most frequent wind direction was from the ENE suggesting that summer 2010 was quite exceptional in respect of wind forcing — according to the long-term wind data, the WSW winds prevail in the region (Keevallik and Soomere 2014). Both, the ENE and WSW winds were frequent during the third deployment in summer 2011 while the average wind speed was 5.7 m s^{-1}. The S and NW winds with mean speed of 7.3 m s^{-1} prevailed during the second (autumn) deployment. The last two measurement periods were characterized by variable weather conditions, with an average wind speed of 9.4 m s^{-1} and 8.5 m s^{-1} (2011/2012 and 2013/2014, respectively). Several storms from SW occurred in December–January 2011/2012 and 2013/2014.

The mean current speed during the autumn 2010 and summer 2011 deployments decreased with the depth, while during the summer 2010 and two winter–spring deployments, currents in the upper and deep layers were slightly stronger than in the intermediate layer (Table 2). The maximum current speed (1 h average) for the

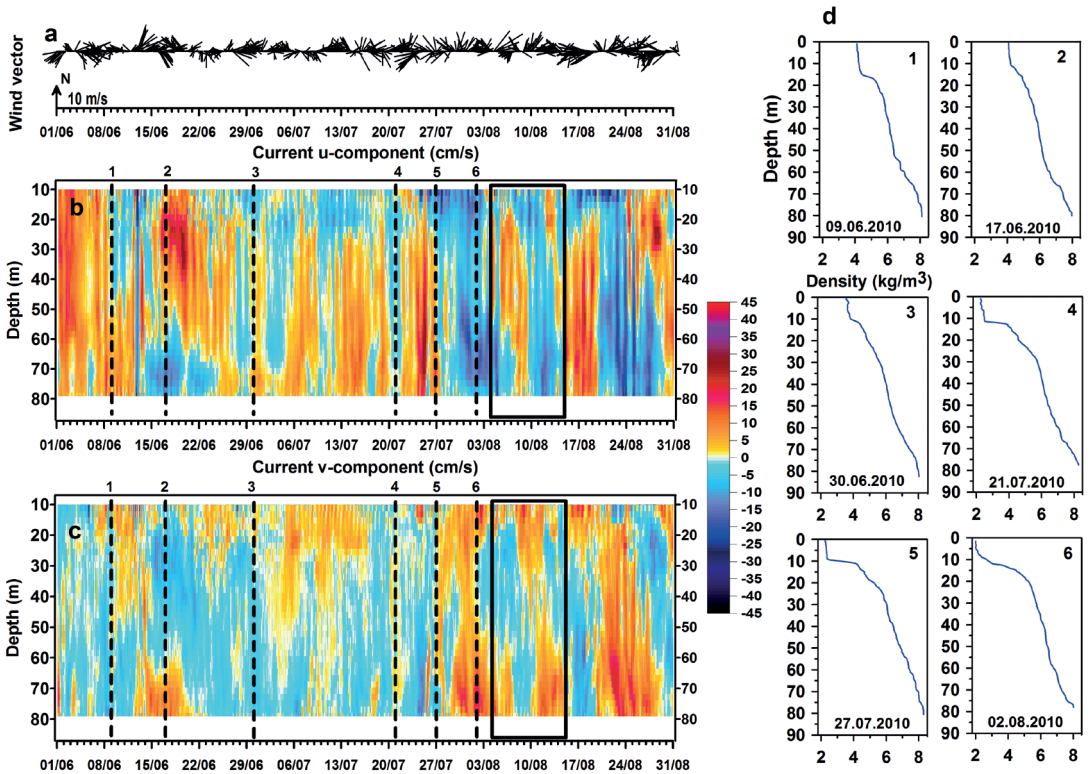

Fig. 2. (**a**) Time series of wind vectors subsampled every 3 h from 1 June to 31 August 2010. The scale is shown by an arrow on the time axis. Time series of the vertical distribution of (**b**) east-west current velocity component (*u*), and (**c**) north–south current velocity component (*v*) for the deployment ADCP1. Vertical dashed lines indicate the CTD measurements presented as (**d**) vertical profiles of density anomaly. The black rectangle indicates the selected period which we analyzed in more detail.

deployments was recorded in the upper layer (the maximum speed was measured in the last week of December 2011) or in the near-bottom layer (the maximum speed was measured on 21 December 2013). An exception was the autumn 2010 measurement period when the maximum current speed was recorded in the intermediate layer.

Summer 2010

Both pycnoclines (the seasonal thermocline and quasi-permanent halocline) were present throughout the first deployment (Fig. 2). A weak barotropic inflow into the gulf (to the east) was observed during the first week of June and a reversal of the estuarine circulation as a reac-

Table 2. Average and maximum values (1 h average) of current speeds (cm s^{-1}) at the five locations.

	Mean speed			Maximum speed		
	Near-bottom layer (m)	Intermediate layer layer (20–50 m)	Upper layer (8–11 m)	Near-bottom layer (m)	Intermediate layer layer (20–50 m)	Upper layer (8–11 m)
ADCP1	8.9 (71–79)	8	11.5	34.9	39.7	55.4
ADCP2	5.6 (54–62)	8.4	10.7	25.8	41.7	35
ADCP3	5.0 (65–73)	7.3	11.1	29.3	23.2	41.3
ADCP4	11.2 (78–86)	9.8	12	36.7	48.9	64.6
ADCP5	11.9 (74–82)	9.7	10.7	58.5	50.6	55.1

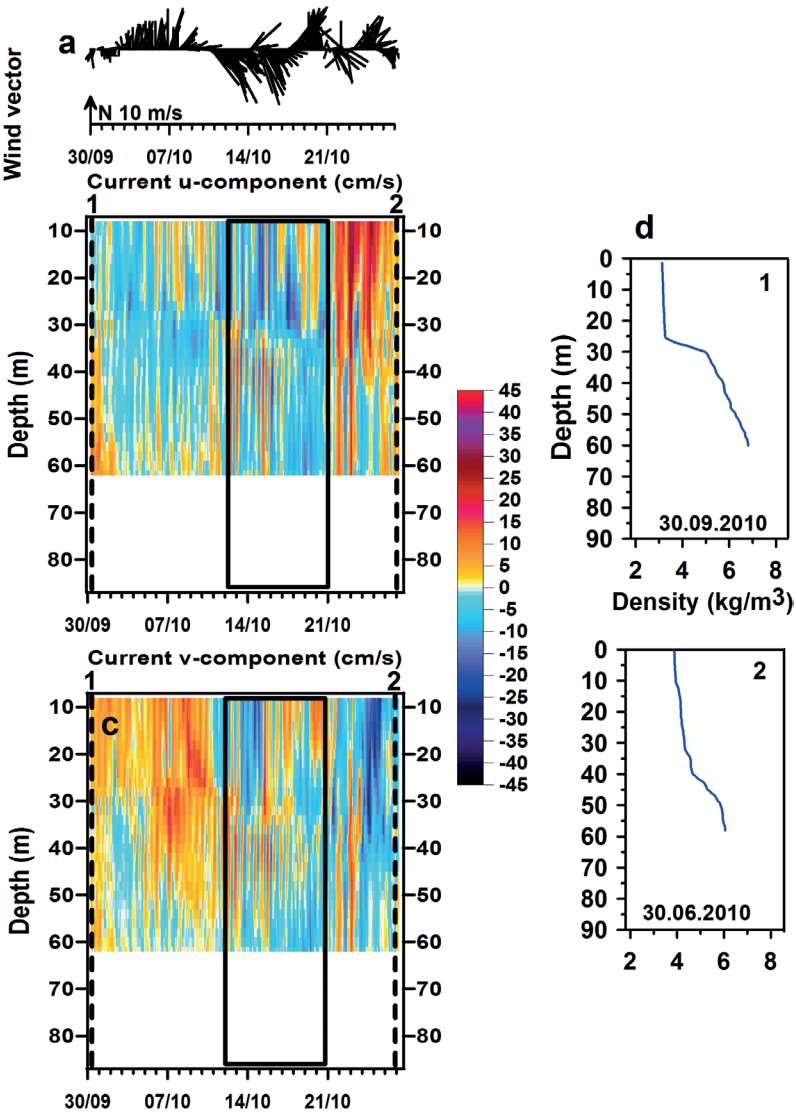

Fig. 3. Same as Fig. 2, but for the deployment ADCP3 from 13 July to 5 September 2011.

tion to the SW wind impulse in mid-June 2010 (Fig. 2). A strong inflow with the current speed exceeding 50 cm s^{-1} in the upper 60 m and an outflow with the maximum speed of 17.2 cm s^{-1} below 60 m depth occurred during this circulation reversal. A relatively weak outflow prevailed in the upper layer, and an inflow was observed beneath the seasonal thermocline in July 2010. Alternating in- and outflow events were observed in the upper and deeper layers in the timescale of about one week as a reaction to the variable wind forcing in August 2010. Strong easterly wind impulses on 23–26 July and 17–19 August 2010 caused strong outflow events (likely upwelling jet along the southern coast) in the upper layer and upwind flow events in the deeper layer.

Summer 2011

Inflow into the gulf dominated in the upper 30 m layer during the second half of July and in the intermediate layer at the beginning of August 2011 (Fig. 3). Starting from 10 August, the flow in the whole water column was rather characterized by an outflow. Current velocities were relatively

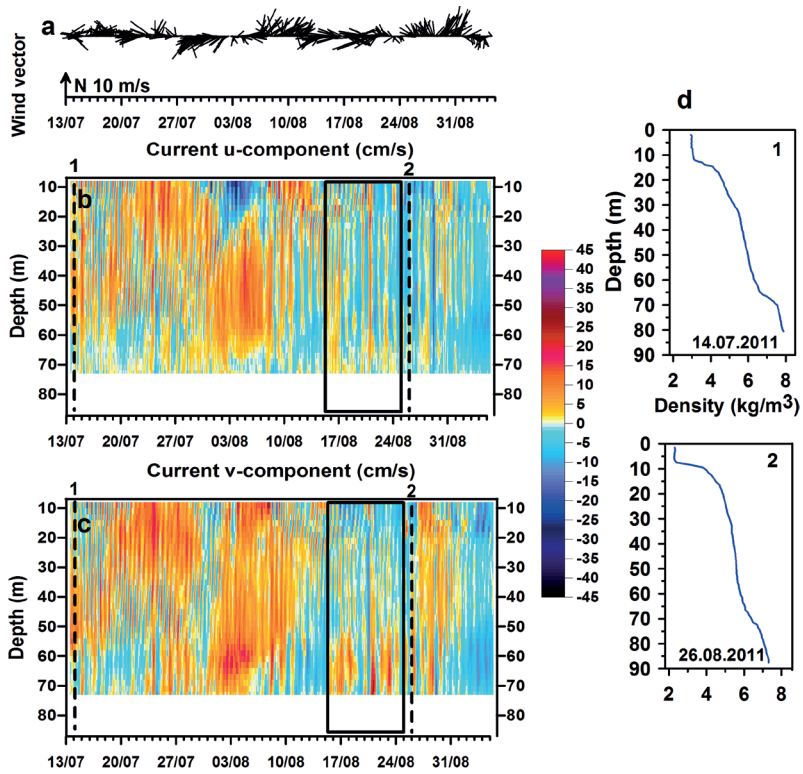

Fig. 4. Same as Fig. 2, but for the deployment ADCP2 from 30 September to 28 October 2010.

weak during this period. A longer period of easterly wind impulse at the end of July caused an outflow from the gulf in the upper 20 m layer at the beginning of August. At the beginning of the observation period and the end of August, both the seasonal thermocline and the quasi-permanent halocline were present in the density profile.

Autumn 2010

The deepest available bin depth (62 m) in the second deployment (Fig. 4) was shallower than the location of the quasi-permanent halocline. However, a strong vertical salinity gradient coincided with the seasonal thermocline. The seasonal thermocline weakened and deepened from the 25–30 m depth to 40–50 m depth during the deployment period. In the first three weeks, an outflow from the gulf prevailed, but rather an inflow dominated during the last week. The flow structure mostly had two layers and the flow separation depth coincided well with the location of the seasonal thermocline.

Winter–spring 2011/2012

The flow during the first month of the fourth observation period had a barotropic structure with alternating in- and outflow events. This structure was a result of the strong south-westerly wind that reversed estuarine circulation and destroyed stratification (Fig. 5). Once stratification vanished, a barotropic flow system formed. In January, the estuarine circulation established due to calm winds and three-layer flow prevailed in the gulf. Another estuarine circulation reversal occurred in February, but in that case, stratification was only weakened, but not collapsed. From March until the end of measurements, a two- or three-layer flow prevailed. Further details of this time-series can be found in the paper by Liblik *et al*. (2013).

Winter–spring 2013/2014

A similar scenario of the variability of the vertical current structure was observed in winter

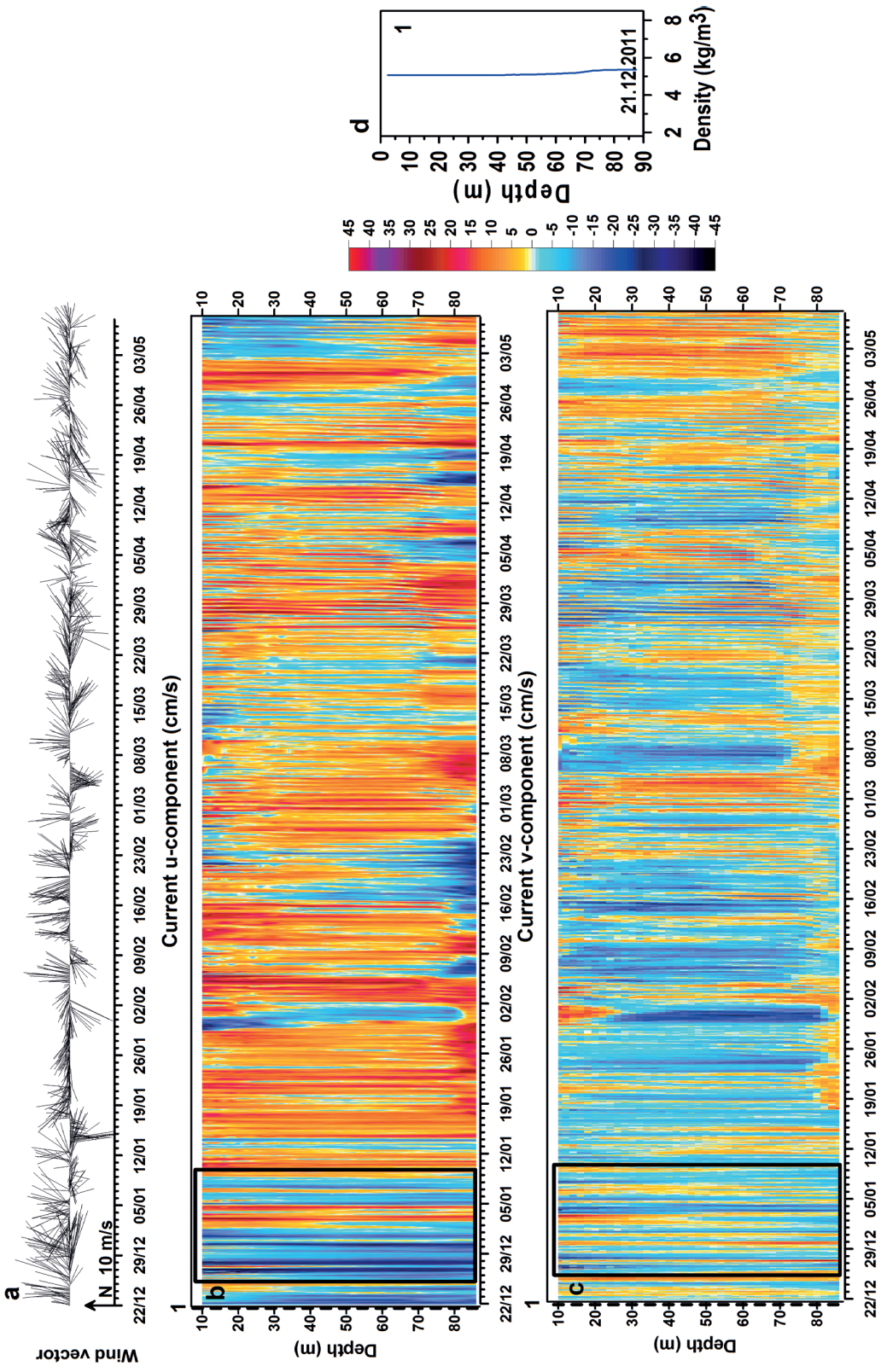

Fig. 5. Same as Fig. 2, but for the deployment ADCP4 from 21 December 2011 to 9 May 2012.

2013/2014. The period from 10 December to 10 January was characterized by a barotropic flow regime due to strong SW-wind domination (Fig. 6). After that, when the wind weakened and turned, first, a barotropic inflow occurred, then a two-layer and later three-layer flow prevailed at the measurement site. Further details can be found in the paper by Lips *et al*. (2017).

Vertical flow structure

Next, we show that one, two or three layers can be distinguished in the vertical current structure in the Gulf of Finland during certain periods. In summer 2010, the current shear was the strongest in the seasonal thermocline (Fig. 7 ADCP1). The other maximum of shear was from time to time observed at the halocline depth, which implies the existence of a three-layer flow in the water column. Similarly to the first observation period, the strongest current shear was observed in the seasonal thermocline in summer 2011 (Fig. 7 ADCP3). The other shear maximum was observed at the depths around 60 m, which was probably associated with the presence of the halocline. Measurements in autumn 2010 showed two-layer flow structure (Fig. 7 ADCP2). During the first half of the observation period, a strong shear maximum was observed at around 25 m depth, and its location deepened due to autumn convection to 40 m by the end of October. The two winter–spring measurements (ADCP4, ADCP5) had a similar pattern of the vertical flow structure (Fig. 7 ADCP4 and ADCP5). The current shear was weak in December and the first half of January. Starting from the second half of January, a strong current shear was present in the halocline. A local shear maximum in the upper layer was associated with the secondary halocline at a depth of 20–25 m.

In order to describe the currents in more detail in the pure one-, two- and three-layer flow cases, periods of 10–17 days were selected (shown by dashed vertical lines in Fig. 7). The number of layers in each period was defined from the period-averaged current shear distribution using the introduced current shear square criterion. The two summer cases (Fig. 8 ADCP1 and ADCP3) revealed a shear minimum in the intermediate layer and maxima in the seasonal thermocline and quasi-permanent halocline. In autumn (Fig. 8 ADCP2), there was a strong shear maximum at mid-depths (30–40 m) that separated the two layers. In two winter cases (Fig. 8 ADCP4 and ADCP5), no clear maxima could be detected. Thus, the flow was mostly barotropic during the two last selected periods. Available density profiles coincide with the average current shear distributions. Stratification strength parameter — the Brunt-Väisälä frequency shows that the water column was almost mixed during the two winter periods. Vertical locations of stronger density stratification in the three other periods — in summers 2010 and 2011 and autumn 2010 roughly match with the current shear maxima.

The directional distribution of currents in each analyzed period is presented by polar histograms (current roses, Fig. 9) at the three depth horizons (the upper layer, intermediate layer, and deep layer) selected based on the existing stratification and current shear maxima. The wind conditions in both typical summer periods were characterized by a variable along-gulf air flow, but the three polar histograms of currents in these periods were rather dissimilar. Northerly current prevailed in the upper layer during the selected period in summer 2010 (ADCP1). In the intermediate layer, the flow was characterized by weak currents either to ESE or WNW, while in the deep layer, the flow was directed to NE. A uniform directional distribution was revealed in the upper layer during the selected period in summer 2011 (ADCP3). The flow in the intermediate layer and the deep layer was dominated by westward and northward currents, respectively. Complex correlation (r) between wind vectors and current vectors revealed high correlation in the upper 9 m layer, being $r = 0.5$ ($n = 89$, $p < 0.01$) for summer 2010 (ADCP1) and $r = 0.7$ ($n = 80$, $p < 0.01$) for summer 2011 (ADCP3).

The NW and south winds dominated during the selected measurement period in autumn 2010 (Fig. 9 ADCP2). The flow in the upper layer and intermediate layer had a uniform distribution of current directions. The flow in the deep layer was dominated by SW currents. The observed similarity of the upper and intermediate layer current roses in the case of the strong mean shear between the layers is explained by the phase shift of cur-

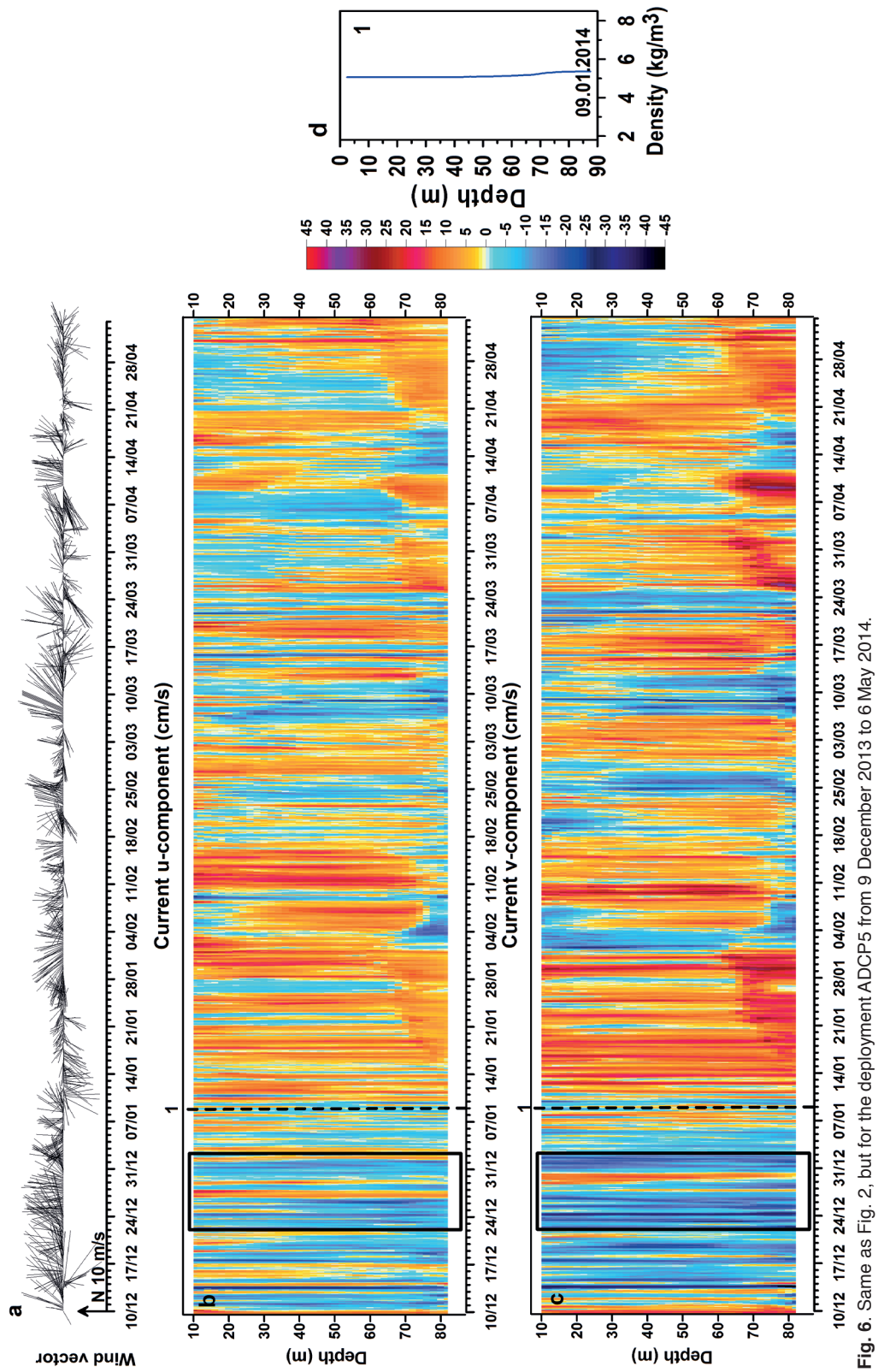

Fig. 6. Same as Fig. 2, but for the deployment ADCP5 from 9 December 2013 to 6 May 2014.

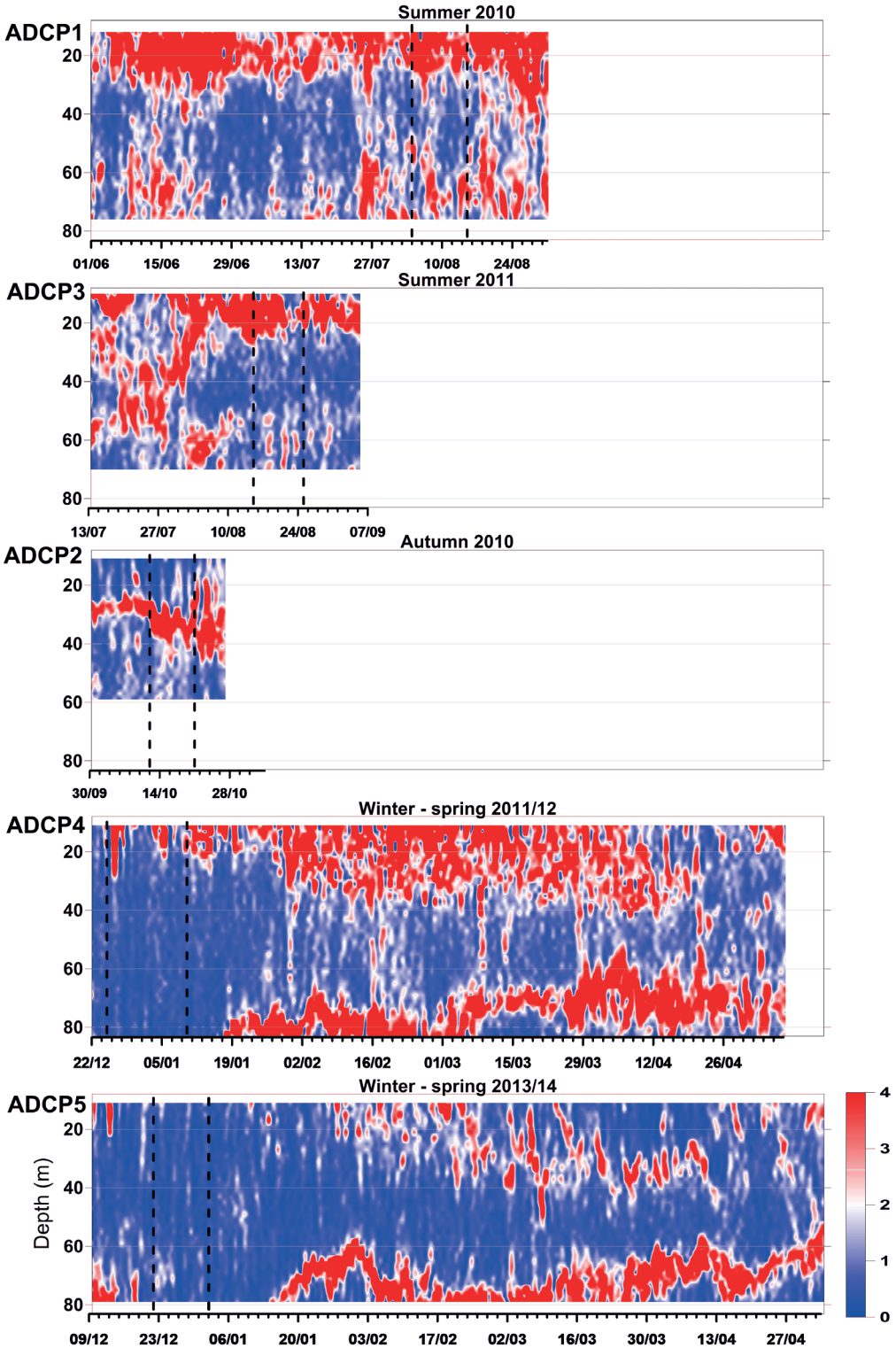

Fig. 7. Low–pass filtered time series of a current shear square (in 10^{-4} s^{-2}) in summer 2010 (ADCP1), summer 2011 (ADCP3), autumn 2010 (ADCP2), winter–spring 2011/2012 (ADCP4), and winter–spring 2013/2014 (ADCP5). Vertical dashed lines indicate the selected periods which we analyzed in more detail.

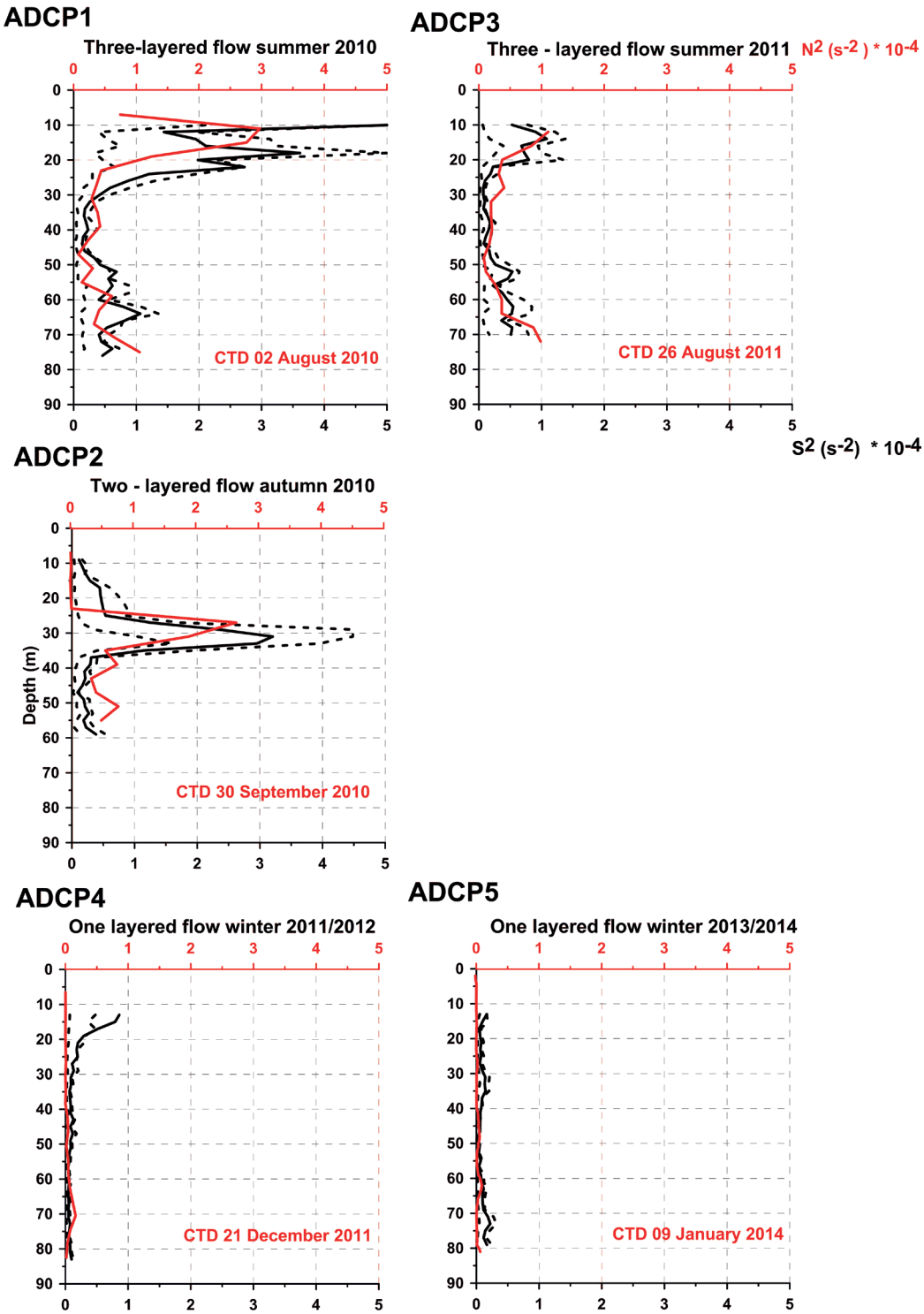

Fig. 8. Median (solid black lines) current shear square (S^2) distribution and typical Brunt-Väisälä frequency square (N^2) profiles (solid red lines) in summer 2010 (ADCP1), summer 2011 (ADCP3), autumn 2010 (ADCP2), winter–spring 2011/2012 (ADCP4), and winter–spring 2013/2014 (ADCP5). Dashed lines indicate 25- and 75-percentiles of the shear.

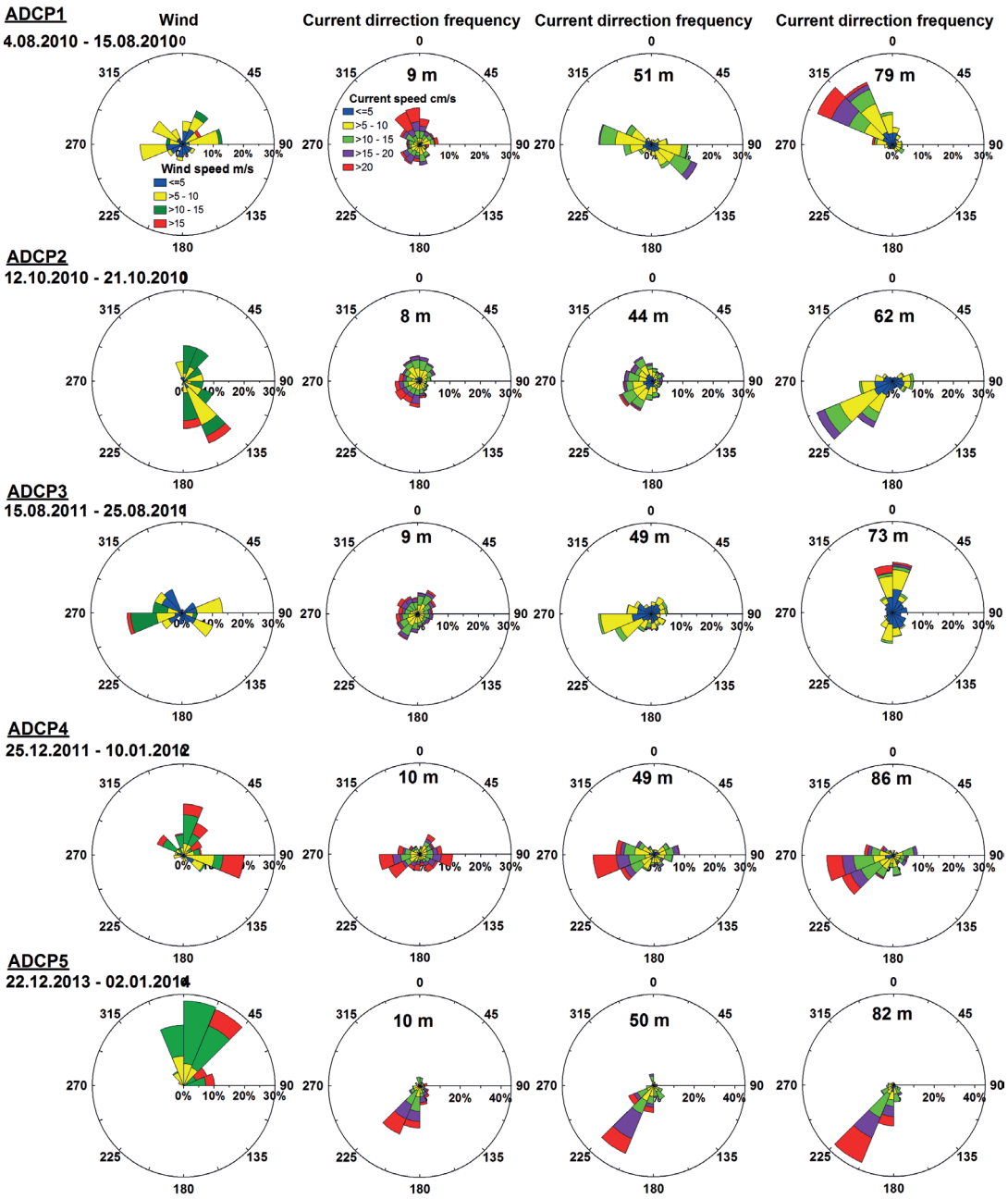

Fig. 9. Wind roses during the five selected periods and current roses at the selected depths in the upper, intermediate, and near-bottom layer. The measured wind direction was turned by 180° to match the wind forcing with the current direction. Colour scales are shown in the first row.

rent oscillations in the pycnocline. Significant vector correlation between the current and wind was found in the sub-surface layer ($r = 0.7$, $n = 73$, $p < 0.001$). The correlation decreased with the depth until it reached a minimum value of $r = 0.5$ ($n = 73$, $p < 0.001$) at the depth of 25 m. Below that depth, the correlation started to grow again reaching a value of $r = 0.8$ at a depth of 34 m.

Both selected winter periods were characterized by strong winds from the southwest. The

current roses in the selected period in winter 2011/2012 (Fig. 9 ADCP4) were rather similar at all depths — the currents to the west dominated in all three layers. In the selected period in winter 2013/2014 (Fig. 9 ADCP5), the up-wind flow directed to the SW was present throughout the water column in this site in the central gulf while a down-wind flow existed near the coast (Lips *et al*. 2017). We suggest that the strong currents during the periods of weak stratification were wind induced since a significant correlation between the wind vectors and current vectors was revealed throughout the water column.

Current velocity spectra

The vertical distribution of kinetic energy throughout the water column was examined for five selected current velocity time series. Similarly to the previous studies, the obtained kinetic energy spectra revealed the energy maxima at the broad semi-diurnal frequency band (BSD), the broad diurnal frequency band (BD), and the low-frequency seiches band (LFS). However, these maxima of kinetic energy were not always present in the spectra in all analyzed periods and depth ranges.

During the two selected periods of one-layer (barotropic) flow structure (25 December 2011–10 January 2012 and 22 December 2013–2 January 2014), high kinetic energy bands were assembled in the range from 21 h to 32 h. Significant peaks were revealed throughout the water column close to the periods of the 1st and 3rd mode seiches in 2011/2012 and the 2nd and 3rd mode seiches in 2013/2014 (Fig. 10 ADCP4 and ADCP5). Energy level recorded for the period close to 1st seiche mode for ADCP4 was higher in the upper layer than in the deeper layers corresponding to a current velocity amplitude of 5.6 cm s^{-1} and 4.6 cm s^{-1}, respectively (current spectrum had 30 degrees of freedom (DoF)). During the selected period in winter 2013/2014, the highest energy level was recorded at a period close to the 2nd seiche mode, with the strongest oscillations in the upper layer and slightly weaker in the intermediate layer, with the amplitude of 7.2 cm s^{-1} and 6.3 cm s^{-1} (DoF = 30), respectively. Hence, during both selected winter periods, strong wind forcing and weak stratification created favorable conditions for the generation of current oscillations with the periods of different mode seiches.

In the selected period of two-layer flow structure from 12 until 21 October 2010, higher spectral energy was concentrated in the broad semi-diurnal frequency band (Fig. 10 ADCP2). The elevated energy was observed from the surface layer to 30 m depth and in the depth range from 36 m to 54 m. Kinetic energy spectra revealed a higher current oscillations amplitude of 8.5 cm s^{-1} (DoF = 30) in the layer below the seasonal thermocline and a lower amplitude of 5.5 cm s^{-1} (DoF = 30) in the upper layer.

Distribution of kinetic energy during the three-layer flow in summer 2010 (4–15 August) showed almost equal energy at the BSD and BD frequencies (Fig. 10 ADCP1). Maximum current oscillations amplitude estimated from the energy spectra in the upper 20-m layer was 5.1 cm s^{-1} for the BSD and 5.5 cm s^{-1} for the BD frequency band (DoF = 30). A prominent BD frequency peak was present in the intermediate layer but was absent at the deepest measurement horizons (at the deepest 20 m). The BSD energy was present throughout the water column, but with very low energy in the depth range from 21 m to 51 m. During the selected period with the three-layer flow structure in summer 2011 (15–25 August), the kinetic energy spectra revealed a clear energy peak in the upper layer at the BSD frequency band and the near-bottom layer at the BD frequency band (Fig. 10 ADCP3) with the current oscillations amplitude of 4.8 cm s^{-1} and 6.1 cm s^{-1}, respectively (DoF = 30). All revealed energy peaks were present in the intermediate layer, but with low energy.

Thus, the current velocity spectra calculated for the selected periods with the quasi-stationary variability of currents revealed clear energy peaks at various frequencies, in the range from BSD to LFS frequencies. During the one-layer flow structure (winter), several modes of seiches close to the 1st, 2nd and 3rd mode were observed. During the two-layer (autumn) and three-layer (summer) flow structure, the temporal variability of currents was influenced by current oscillations belonging to the broad semi-diurnal and broad diurnal frequency bands.

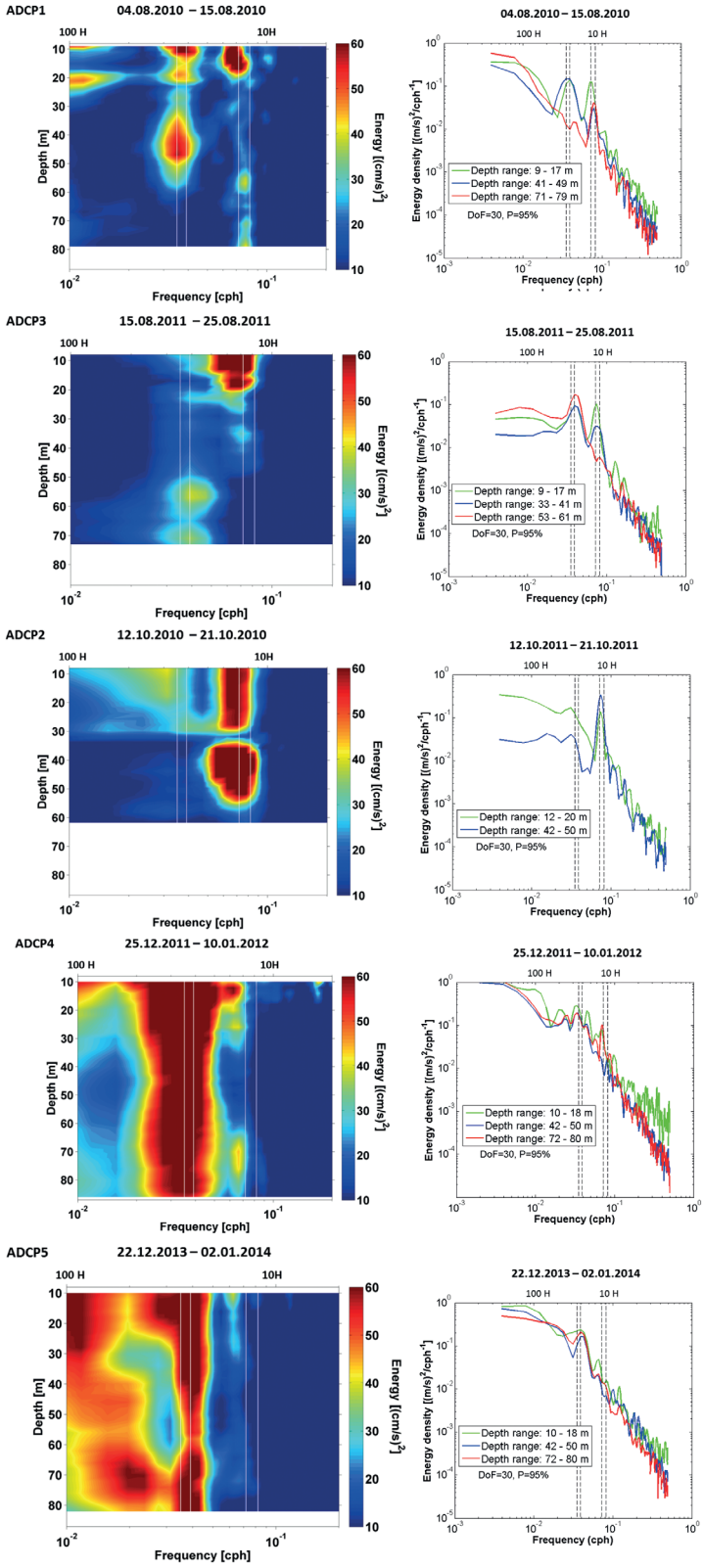

Fig. 10. (Left column) Vertical distributions of kinetic energy spectra during three-layer flow (ADCP1, ADCP3), two-layer flow (ADCP2), and one-layer flow (ADCP4, ADCP5). (Right column) Depth-averaged kinetic energy density for the upper, intermediate, and near-bottom layer. Vertical white lines (left column) and dashed lines (right column) indicate the oscillation periods of 28.6 h, 25.6 h, 13.9 h, and 12.42 h.

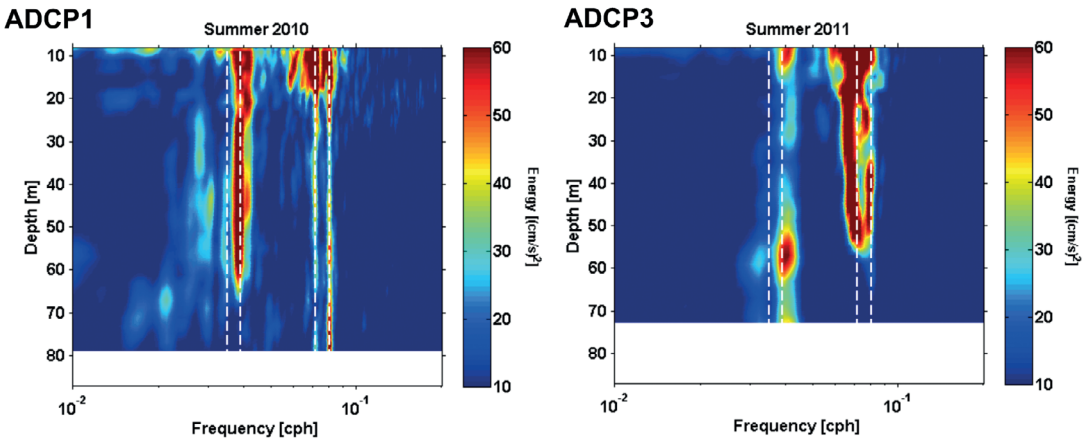

Fig. 11. Vertical distribution of kinetic energy spectra in summer 2010 (ADCP1) and summer 2011 (ADCP3). Vertical dashed lines indicate the oscillation periods of 28.6 h, 25.6 h, 13.9 h, and 12.42 h.

The current velocity spectra for the selected periods from summers 2010 and 2011 revealed the energy peaks at similar frequencies. However, the BD frequencies had higher energy from the surface to 60 m depth in summer 2010, while in summer 2011, these frequencies had a higher energy in the halocline and below it. The second discrepancy between these two summer periods was within the range of BSD frequency. An energy peak at this frequency was present in the whole water column in the selected period from summer 2010 while it was distinguishable only in the upper 50 m in summer 2011. In order to verify if this disparity existed for the whole time-series acquired in summers 2010 and 2011, we calculated the kinetic energy spectra for both full measurement periods.

Current velocity spectra for summer 2010 showed that the most pronounced peaks for the 15-m-thick upper layer were found in the range of oscillation periods from 12 to 27 h (Fig. 11 ADCP1). The M_2 semidiurnal tidal period was present through the whole water column. A prominent spectral maximum at a period close to the local inertial oscillation period (13.9 h) had higher energy in the upper 50 m depth. Energy maxima at the BD frequency band were found in the upper 60 m depth with the almost same energy level, but this peak was not distinguishable in the near-bottom layer.

Similarly, prominent spectral maxima were found for summer 2011 in the period interval from 12.3 to 18 h and at a period close to the 2nd mode seiches. The broad semi-diurnal frequencies had higher energy in the upper layer if compared to the intermediate layer and did not reveal an energy maximum in the deepest 20-m-thick layer. The prominent peak at a period close to the 2nd mode seiches was present throughout the water column. The kinetic energy spectra revealed more energetic oscillations in the upper layer (upper 10 m) and near-bottom layer, but there was less energy in the layer from 15 to 40 m (Fig. 11 ADCP3).

Thus the two spectra calculated from the full data sets support the mismatch of vertical distributions of kinetic energy spectra between the two selected time-series in summers 2010 and 2011.

Discussion

The analyzed five current measurement time-series revealed that one-, two- or three-layer current structure could occur in the Gulf of Finland depending on the wind forcing and stratification. If we consider the Baltic Sea as an estuarine system, it can be classified as a strongly stratified estuary based on freshwater flow and mixing parameters (Geyer and MacCready 2014). The elongated Gulf of Finland has the main freshwater source at its eastern end and free water exchange with the Baltic Proper through its western border (Alenius *et al*. 1998). Thus, the gulf can be considered as an estuary of the Baltic

Sea. Our results show that the Gulf of Finland is rather extraordinary among world estuaries (Geyer and MacCready 2014) since it can switch from one- to three-layer flow system over time. Likewise, in that respect, the Gulf of Finland is unique in the Baltic Sea. The shallower areas of the Baltic (e.g., the Gulf of Riga and the Belt Sea) operate as one- or two-layer systems (e.g., Lilover *et al*. 1998, Jakobsen and Trebuchet 2000) while in the central Baltic two- and three-layer flow regimes exist (Lass *et al*. 2003).

The most common current structure had two shear maxima and, thus, mostly the three-layer flow occurred in the gulf. As it was also noticed in the earlier studies, the current shear maxima coincide with the two pycnoclines: seasonal thermocline (e.g., Suhhova *et al*. 2015) and quasi-permanent halocline (e.g., Liblik *et al*. 2013). This feature can be confirmed by the time-series acquired during all deployments analyzed in the present study. Strong current shear was also often observed at 10–20 m depth in winter 2011/2012 when the seasonal thermocline did not exist. This shear maximum appeared in the periods of easterly winds that initiated westward transport of fresher water in the upper layer and, in turn, created vertical salinity gradient at the depths of 10–20 m, as also noted by Liblik *et al*. (2013). The advection of fresher water is clearly distinguished in the vertical section of the salinity (e.g., Liblik *et al*. 2013: fig. 3) and current shear (Fig. 7). Similar surface layer current can be detected based on the long-term measurements near the northern coast in the entrance area of the gulf (e.g., Rasmus *et al*. 2015: fig. 5). While the latter observation agrees with the classical concept of the cyclonic circulation scheme in the gulf (Palmén 1930, Alenius *et al*. 1998), we suggest that the fresher surface current can also be observed in the deeper central and southern parts of the gulf (Fig. 5).

The presented current roses confirm that the currents and their variability were similar throughout the water column under conditions of strong up-estuary wind forcing and weak stratification (Fig. 9 ADCP4 and ADCP5). However, the down-estuary current was more persistent in the deeper layers than in the upper layer, as it was expected in the central, deeper part of the gulf where the flow was up-wind. For one of these analyzed winter periods (from winter 2013/2014), a strong down-wind (up-estuary) current was observed along the southern coast at the same time (Lips *et al*. 2017). We assume that two-cell circulation was observed in the study period, which is typical in semi-enclosed basins or lakes (Sanay and Valle-Levinson 2005, Winant *et al*. 2014). During the reversal of estuarine circulation, the up-wind barotropic flow appeared along the thalweg and downwind barotropic flow along the shores (Lips *et al*. 2017).

The current roses qualitatively differed between the layers in the stratified conditions (Fig. 9 ADCP1, ADCP3, and ADCP2). The currents were directionally more equally distributed in the upper layer for the selected summer periods and both the upper and the intermediate layer in autumn. The observed narrow current roses in the deepest layer imply that the currents were topographically steered. A shallow area (Uusmadal) is located to the southeast from the ADCP1 deployment site, and the ADCP3 was deployed in a deeper area between the bottom elevations with the depth of 55–60 m to the east and west from the measurement site. The latter explains the observed discrepancy between the orientation of the gulf and near-bottom currents at ADCP3. This result together with observations by Lilover *et al*. (2017) suggests that channel-like flow in the near bottom layer is a typical feature of the Gulf of Finland.

The prominent spectral peaks at periods from 12.4 h to 26 h (summer measurements) and 14 h to 31 h (winter measurements) indicate the current oscillations due to seiches, tides, and inertial currents. These peaks in the current velocity spectra comprise the local inertial period (13.9 h) and semidiurnal (12.42 h) and diurnal (25.8 h) tidal period (Lilover 2012), as well as seiches-driven current oscillation periods of 16 h (Lilover 2011), 23 h (Jönsson 2008), 26.4 h, and 31 h (Wübber and Krauss 1979). While prominent peaks close to the inertial frequency were found in the upper and intermediate layers during two-layer flow structure in October 2010, they were almost absent in winter. We assume that the presence of strong seiches and absence of inertial oscillation during one-layer flow can be caused by stormy weather conditions in the study area during our selected periods (Liblik *et al*. 2013, Lips *et al*. 2017).

Wind forcing and disappearance of vertical stratification created favorable conditions for seiche-induced oscillations in the study area (Breaker *et al*. 2010, Simpson *et al*. 2014). Under created conditions, the oscillations are expected to be stronger during winter and autumn periods (Alford *et al*. 2012, Simpson *et al*. 2014). Barotropic flow system was observed during these winter periods, which could cause the absence of inertial oscillations, because of their baroclinic nature (Maas and van Haren, 1987). Furthermore, the kinetic energy spectra revealed the presence of oscillations at the BSD frequencies in the middle of January 2014 after the wind subsided and layered flow structure occurred. The presence of near-inertial oscillations was associated with the re-establishment of stratification (Shearman 2005, Rabinovitch, 2009Castillo *et al*. 2017).

The current velocity spectra for summer periods also showed that the temporal variability of currents (in the range of periods from 12.4 to 26 h) is highly influenced by inertial oscillations, seiches, and tides. In summer 2010, the BD band energy was at a high level from the surface layer to the halocline while this local peak of energy was absent in the near-bottom layer. At the same time, the BSD band energy peak was present in the entire water column from the surface to the near-bottom layer. In summer 2011, the vertical distribution of kinetic energy in these frequency bands were reversed. The BD band energy had high values also in the near bottom layer and BSD band energy being high from the surface to the halocline had no peak in the near-bottom layer (Fig. 11 ADCP1 and ADCP3).

In order to explain the above-mentioned discrepancy between the two summers, we calculated kinetic energy spectra of currents measured in summers 2009 and 2012 at sites very close to the first deployment in 2010. The current velocity spectra showed similar results for the three summer measurements made in the same location (2009, 2010 and 2012 measurements). We suggest that the near-bottom layer was partly disconnected from the above flow structure in summer 2011 due to the topographic peculiarities of the exact measurement site. It can also be qualitatively seen from the current roses (Fig. 9) as an altered orientation of the near-bottom currents and more persistent current direction in the intermediate layer in summer 2011, which is similar to the persistency of currents in the deep, near-bottom layer during the other measurements in stratified conditions (summer and autumn 2010). However, further studies are needed to see if different current spectra for the 2011 measurements are a sign of regular geographical feature as the measurements were conducted at the rim area 17 km north of the site of the other summer measurements.

The estimated kinetic energy spectra of currents for winter 2013/2014 and both summer measurements revealed significant peaks with the period close to the 2nd seiche mode. This peak could also be related to the diurnal tide period (O_1 25.8 h), as mentioned by Lilover (2011 and 2012). We assume that strong oscillations close to this local energy maximum period could be a combination of these two energy sources. However, the role of tidal forcing in vertical mixing is considered to be low in the Baltic Sea in comparison with the water bodies under tidal influence (Reissmann *et al*. 2009, Valle-Levinson *et al*. 2014). Similarly to the smaller lakes (Lorke *et al*. 2002) and fjords (Arneborg and Liljebladh 2001) with low tidal forcing, seiches, and inertial oscillations have a relatively higher contribution in vertical mixing in the Baltic Sea. It is shown (e.g., Lappe and Umlauf 2016) that the near-inertial waves together with topographic waves are the dominant motions that trigger vertical mixing in the bottom boundary layer in the central Baltic Sea. The contribution of such mixing at the sloping bottoms is suggested to be the main contributor to Baltic deep water mixing (Holtermann *et al*. 2012).

Theoretical studies on the influence of vertical mixing due to current oscillations and its lateral variability (e.g., due to topography) on the transverse structure of residual circulation have mostly considered tidal current oscillations as the energy source (Burchard *et al*. 2011, Winant *et al*. 2014). The comparison of vertical stability and current shear (Fig. 8) indicates that even though the estimated amplitudes of current oscillations at different prevailed frequency bands are relatively low (order of 5 cm s^{-1}), the mixing events might frequently occur. Furthermore, as identified by Lips *et al*. (2017), the average

current speed was clearly higher in the coastal area than in the deepest part of the gulf when the barotropic flow structure was established in winter 2013/2014. Thus, the lateral gradient in mixing effects, which in turn influences the residual flow structure, could exist in the Gulf of Finland. However, further studies are needed to quantify the mixing effects and their impact on the circulation scheme in the gulf.

We showed that the characteristics of kinetic energy spectra are linked to the density structure of the water column. For BSD frequency band, the measurement ADCP2 is a good example of the link between the density field (Fig. 8 ADCP2) and kinetic energy spectrum (Fig. 10 ADCP2 left column). Therefore, the changes in thermohaline structure at different time-scales (decadal, seasonal, and synoptic) should also appear in kinetic energy spectra in different water layers. For instance, one could expect that the vertical distribution of current spectra in the Gulf of Finland before the Major Baltic Inflow in 1993 (Matthäus and Lass 1995) were similar to the two-layer structure due to much weaker stratification through the halocline (Liblik and Lips 2011). It also means that if we observe warmer but stormy winters (as in winter 2014/2015; see Uotila *et al*. 2015) in future, the one-layer flow system realizes more often in the gulf.

Concluding remarks

The analyzed current measurements revealed the occurrence of barotropic and layered flow structures in the Gulf of Finland. The layered flow structure emerged as both the local shear maxima in certain layers and the differences in the kinetic energy spectra of currents between the vertical layers. We confirmed that the location of shear maxima of current velocity is strongly linked to the pycnoclines, including the vertical salinity gradient appearing in the upper 10–20 m layer under certain flow structure in the absence of the seasonal thermocline in winter. The main energy source of the motions in the gulf is wind. The energy maxima of current oscillations occurred at a broad semi-diurnal frequency band, broad diurnal frequency band, and low-frequency seiches band, as it has also been found earlier in the Gulf of Finland. The frequency composition differed between the seasons mainly due to the vertical stratification, as well as between the layers during a selected period. The kinetic energy spectra of currents in the periods of strong wind forcing and weak stratification were dominated by current oscillations throughout the water column coinciding with different modes of seiches. During the periods of the two- or three-layer residual flow also inertial oscillations and probably tides remarkably contributed to the kinetic energy of current oscillations. We demonstrated that in summer, the inertial oscillations were dominating in the upper layer from the surface to either the thermocline or the halocline. Seiches had higher energy from the surface to 60 m depth in summer 2010, while in summer 2011, they had higher energy in the quasi-permanent halocline and below (it must be noted that the measurements were conducted at different locations).

Acknowledgements: The work was supported by institutional research funding (IUT19-6) of the Estonian Ministry of Education and Research. The measurements and analysis were partly funded by the Estonian Ministry of Environment (Nord Stream construction environmental monitoring) and Estonian Science Foundation grants no. 6955, 9023, and 9382. We thank our colleagues and the crew of the research vessel Salme for their help at sea.

References

Alenius P., Myrberg K. & Nekrasov A. 1998. The physical oceanography of the Gulf of Finland: a review. *Boreal Env. Res.* 3: 97–125.

Alford M.H., Cronin M.F. & Klymak J.M. 2012. Annual Cycle and Depth Penetration of Wind Generated Near-Inertial Internal Waves at Ocean Station Papa in the Northeast Pacific. *Journal of Oceanography* 42: 889–909.

Andrejev O., Myrberg K., Alenius P. & Lundberg P.A. 2004. Mean circulation and water exchange in the Gulf of Finland — a study based on three-dimensional modeling. *Boreal Env. Res.* 9: 1–16.

Arneborg L. & Liljebladh B. 2001. The internal seiches in Gullmar Fjord. Part II: Contribution to Basin Water Mixing. *J. Phys. Oceanogr.* 31: 2567–2574.

Bennet J.R. 1974. On the dynamics of wind-driven lake currents. *J. Phys. Oceanogr*. 4: 400–414.

Bergström S. & Carlsson B. 1994. River runoff to the Baltic Sea: 1950–1990. *Ambio* 23: 280–287.

Book J.W., Perkins H., Signell R.P. & Wimbush M. 2007. *The Adriatic Circulation Experiment winter 2002/2003*

mooring data report: A case study in ADCP data processing. Rep. NRL/MR/7330-07-8999, U.S. Naval Res. Lab., Stennis Space Center, MS.

Burchard H., Hetland R.D., Schulz E. & Schuttelaars H.M. 2011. Drivers of residual estuarine circulation in tidally energetic estuaries: straight and irrotational channels with parabolic cross section. *J. Phys. Oceanogr*. 41: 548–570.

Butterworth S. 1930. On the theory of filter amplifiers. *Experimental Wireless and the Wireless Engineer* 7: 536–541.

Breaker L.C., Tseng Y.-H. & Wang X. 2010. On the natural oscillations of Monterey Bay: Observations, modeling, and origins. *Progress in Oceanography* 86: 380–395.

Castillo I.M., Pizarro O., Ramírez N. & Cáceres M. 2017. Seiche excitation in highly stratified fjord of southern Chile: the Reloncaví fjord. *Ocean Sci*. 13: 145–160.

Elken J., Raudsepp U. & Lips U. 2003. On the estuarine transport reversal in deep layers of the Gulf of Finland. *J. Sea Res*. 49: 267–274.

Elken J., Nõmm M. & Lagemaa P. 2011. Circulation patterns in the Gulf of Finland derived from the EOF analysis of model results. *Boreal Env. Res*. 16: 84–102.

Elken J., Raudsepp U., Laanemets J., Passenko J., Maljutenko I., Pärn O. & Keevallik S. 2014. Increased frequency of wintertime stratification collapse events in the Gulf of Finland since the 1990s. *Journal of Marine Systems* 129: 47–55.

Emery W.J. & Thomson R.E. 2004. *Data analysis methods in physical oceanography*. Elsvier, London, UK.

Geyer W.R. & MacCready P. 2014. The estuarine circulation. *Annu. Rev. Fluid Mech*. 46: 175–197.

Holtermann P., Umlauf L., Tanhua T., Schmale O., Rehder G. & Waniek J. 2012. The Baltic Sea tracer release experiment. 1. Mixing rates. *J. Geophys. Res*. 117, C01021, doi:10.1029/2011JC007439.

Jakobsen F. & Trébuchet C. 2000. Observations of the transport through the belt sea and an investigation of the momentum balance. *Cont. Shelf Res*. 20: 293–311.

Jönsson B., Döös K., Nycander J. & Lundberg, P. 2008. Standing waves in the Gulf of Finland and their relationship to the basin-wide Baltic seiches. *J. Geophys.Res*. 113, C03004, doi:10.1029/2006JC003862.

Keevallik S. & Soomere T. 2014. Regime shifts in the surface-level average air flow over the Gulf of Finland during 1981–2010. *Proceedings of the Estonian Academy of Sciences* 63: 428–437.

Kundu P.K. 1976. Ekman veering observed near the ocean bottom. *J. Phys. Oceanogr*. 6: 238–242.

Lappe C. & Umlauf L. 2016. Efficient boundary mixing due to near-inertial waves in a nontidal basin: observations from the Baltic Sea. *J. Geophys. Res. Oceans* 121: 8287–8304.

Lass H.-U., Prandke H. & Liljebladh B. 2003. Dissipation in the Baltic Proper during winter stratification. *J. Geophys. Res.* 108(C6), 3187, doi:10.1029/2002JC001401.

Launiaine J. & Saarinen J. 1984. Marine wind characteristics in the northern Baltic Sea. *Finnish Mar. Res.* 250: 52–86.

Liblik T. & Lips U. 2011. Characteristics and variability of the vertical thermohaline structure in the Gulf of Finland in summer. *Boreal Env. Res*. 16 (suppl. A): 73–83.

Liblik T. & Lips U. 2012. Variability of synoptic-scale quasi-stationary thermohaline stratification patterns in the Gulf of Finland in summer 2009. *Ocean Science* 8: 603–614.

Liblik T., Laanemets J., Raudsepp U., Elken J. & Suhhova I. 2013. Estuarine circulation reversals and related rapid changes in winter near-bottom oxygen conditions in the Gulf of Finland, Baltic Sea. *Ocean Science* 9: 917–930.

Liblik T. & Lips U. 2017. Variability of pycnoclines in a three-layer, large estuary: the Gulf of Finland. *Boreal Env. Res*. 22: 27–47.

Lilover M.-J., Lips U., Laanearu J. & Liljebladh B. 1998. Flow regime in the Irbe Strait. *Aquat. Sci*. 60: 253–265.

Lilover M.-J., Pavelson J., Kõuts T. 2011. Wind forced currents over the shallow Naissaar bank in the Gulf of Finland. *Boreal Env. Res*. 16: 164–174.

Lilover M.-J. 2012. Tidal currents as estimated from ADCP measurements in "practically non-tidal" Baltic Sea. In: *Baltic International Symposium (BALTIC)*, IEEE/OES, Klaipeda, Lithuania, pp. 1–4.

Lilover M.-J., Elken J., Suhhova I. & Liblik T. 2017. Observed flow variability along the thalweg, and on the coastal slopes of the Gulf of Finland, Baltic Sea. *Estuarine Coastal and Shelf Science*. 195: 23–33.

Lips U., Laanemets J., Lips I., Liblik T., Suhhova I. & Suursaar Ü. 2017. Wind-driven residual circulation and related oxygen and nutrient dynamics in the Gulf of Finland (Baltic Sea) in winter. *Estuarine Coastal and Shelf Science* 195: 4–15.

Lorke A., Umlauf L., Jonas T. & Wüest A. 2002. Dynamics of turbulence in low-speed oscillating bottom-boundary layers of stratified basins. *Environmental Fluid Mechanics* 2: 291–313.

Maas L.R.M. & van Haren J.J.M. 1987. Observations on the vertical structure of tidal and inertial currents in the central North Sea. *J. Mar. Res*. 45: 293–318.

Matthäus W. & Lass H.-U. 1995. The recent salt inflow into the Baltic Sea. *J. Phys. Oceanogr*. 25: 280–286.

Palmén E. 1930. Untersuchungen über die Strömungen in den Finland umgebenden Meeren. *Soc. Sci. Fenn. Comm. Phys.-Math*. 5: 1–94.

Rabinovich A. 2009. Seiches and Harbor Oscillations. In: Kim Y. (ed.), *Handbook of Coastal and Engineering*, World Scientific Publishing Co., California State University, Los Angeles, CA, pp. 193–236.

Rasmus K., Kiirikki M. & Lindfors A. 2015. Long-term field measurements of turbidity and current speed in the Gulf of Finland leading to an estimate of natural resuspension of bottom sediment. *Boreal Env. Res*. 20: 735–747.

Reissmann J., Burchard H., Feistel R., Hagen E., Lass H.-U., Mohrholz V., Nausch G., Umlauf L. & Wieczorek G. 2009. Vertical mixing in the Baltic Sea and consequences for eutrophication: A review. *Progr. Oceanogr*. 82: 47–80.

Sanay R. & Valle-Levinson A. 2005. Wind-induced circulation in semienclosed homogeneous, rotating basins. *J. Phys. Oceanogr*. 35: 2520–2531.

Shearman R.K. 2005. Observations of near-inertial current variability on the New England shelf. *J. Geophys. Res.*

110, C2, C02012, doi:10.1029/2004JC002341.

Simpson J.H., Lucas N.S., Powel B. & Maberly S.C. 2014. Dissipation and mixing during the onset of stratification in a temperate lake, Windermere. *Limnol. Oceanogr*. 60: 29–41.

Suhhova I., Pavelson J. & Lagemaa P. 2015. Variability of currents over the southern slope of the Gulf of Finland. *Oceanologia*. 57: 132–143.

Uotila P., Vihma T. & Haapala J. 2015. Atmospheric and oceanic conditions and the extremely low Bothnian Bay sea ice extent in 2014/2015. *Geophys. Res. Lett*. 42: 7740–7749.

Valle-Levinson A., Cacares M.A. & Pizarro O. 2014. Variations of tidally driven three-layer residual circulation in fjords. *Ocean Dyn.* 64: 459–469.

Winant C., Valle-Levinson A., Ponte A., Winant C., Gutierrez-de-Velasco G. & Winters G. 2014. Observations on the lateral structure of wind-driven flows in a stratified, semiarid bay of the Gulf of California. *Estuaries and Coasts*. 37: 1319–1328.

Wübber C. & Krauss W. 1979. The two-dimensional seiches of the Baltic Sea. *Oceanol. Acta* 2: 435–446.